Sensors and Materials, Vol. 35, No. 3 (2023) 1069–1080
MYU Tokyo

S & M 3229

Characteristics and Application of Zinc Oxide/Magnesium Oxide Hybrids

I-Po Tai,[1] Kuo-Chin Hsu,[1] I-Tseng Tang,[2] Te-Hua Fang,[1*] Tsung-Chieh Cheng,[1] Wei-Hao Wang,[2] Mustufa Ali Ansari,[1] and Chi-Jen Shih[3]

[1]Department of Mechanical Engineering, National Kaohsiung University of Science and Technology, No. 415, Jiangong Rd., Sanmin Dist., Kaohsiung City 807618, Taiwan
[2]Department of Greenergy, National University of Tainan, 33, Sec. 2, Shu-Lin St., Tainan City 700301, Taiwan
[3]Department of Fragrance and Cosmetic Science, College of Pharmacy, Kaohsiung Medical University, No. 100, Shih-Chuan 1st Road, Sanmin Dist., Kaohsiung City 80708, Taiwan

(Received July 26, 2022; accepted March 1, 2023)

Keywords: photocatalysis, ZnO, MgO, methylene blue, methyl orange

In this paper, we discuss the degradation characteristics of methylene blue and methyl orange after being mixed with zinc oxide (ZnO) and magnesium oxide (MgO) powders. Five types of ZnO/MgO mixed powders with different molar ratios (ZnO:MgO molar ratios of 0.95:0.05, 0.9:0.1, 0.85:0.15, 0.8:0.2, and 0.75:0.25) and two different catalyst concentrations were used in the experiment. Catalyst concentrations of 0.5 and 0.15 g/L were used to degrade methylene blue and methyl orange, respectively. The results showed that the powder with a molar ratio of 0.9:0.1 had a high degradation efficiency when the catalyst concentration was 0.15 g/L. The degradation of methyl orange was completed within 6 h, and the degradation of methylene orange reached 80% within 2 h.

1. Introduction

The photocatalytic degradation of organic materials is an efficient approach to the analysis of wastewater containing organics.[1–5] This process presents a perfect opportunity to use solar light energy for degradation.[6–9] However, the amount of visible light energy used for photocatalytic reactions is very small.[10,11] Some researchers use band gap engineering and atomic doping procedures to alter the size of the energy differences between the ground and excited states and the energy of the absorption band of visible light to enhance photocatalytic efficiency.[12–14] In addition, a study has shown that impurities can act as carrier traps and prolong the lifetime of photogenerated carriers.[15] The addition of heterostructures can be a type of bandgap engineering, and in many studies, heterostructures are used to prepare materials for treatment.[16–19] After combining two different materials, owing to changes in work function, photoelectrons and holes may be transferred after their regeneration, reducing the recombination rate of electron holes,[20,21] increasing the stability of the materials, and improving photocatalytic efficiency. [22,23]

*Corresponding author: e-mail: fang@nkust.edu.tw
https://doi.org/10.18494/SAM4233

ISSN 0914-4935

Zinc oxide is a semiconductor material with a wide energy gap and is often used in optoelectronic components, gas sensing, and photocatalysis.[24–28] In the field of photocatalysis, different materials have been used to dope a base material to improve its catalytic capacity.[29–31] For example, bismuth-containing materials have a small energy gap and may be combined with other substances to generate a larger energy gap. Such materials can efficiently expand the visible light band of zinc oxide.[32,33] Zarezadeh *et al.* used BiOBr and AgBr to dope ZnO materials and found that the degradation capabilities of ZnO/BiOBr/AgBr and ZnO/BiOBr materials were 95.3 and 3 times that of pure zinc oxide, respectively.[34] Hanh *et al.* used copper doping to generate carrier traps, and a Cu/ZnO photocatalyst with a weight ratio of 3 wt% demonstrated the highest microchannel plate (MCP) efficiency in the degradation of phosphorus-containing pesticides. [35] Doping with precious metals (Au, Ag, Pt, and Pd) prevents electron recombination through electron transfer. [36–38] Liu *et al.* used a two-step procedure to form Ag–ZnO photocatalysts and found that 3 mol% Ag doping provides the highest photocatalytic efficiency.[39] In addition, nonmetals are also considered to be good doping materials.[40–42]

From these studies, it can be seen that photogenerated carriers greatly affect photocatalytic reactions.[43] MgO is also a common additive to such materials. Panchal *et al.* used substances taken from plants to synthesize ZnO/MgO nanocomposites (NCs)[44] and found that they have excellent antibacterial activity. Sangeeta *et al.* used the solution combustion method to synthesize ZnO/MgO (1:1) composite materials with oxalyl hydrazide as fuel; these materials exhibited a higher catalytic ability for incocyanine (IC) dyes under UV light than pure MgO and ZnO.[45] In this experiment, ZnO/MgO powders with different molar ratios were mixed and investigated for their photocatalytic properties. Scattered energy spectrometry, scanning electron microscopy (SEM), X-ray diffractometry, UV-visible spectrometry, and other techniques were used to examine powders with distinct molar ratios.

2. Materials and Methods

The chemicals used in the experiment include ZnO powder and MgO particles as photocatalytic materials, and methylene blue and methyl orange were used as organic contaminants for photocatalysis experiments.

ZnO/MgO hybrid powders were prepared using the vibration-milled solid-state reaction method. Appropriate amounts of ZnO and MgO powders were mixed at different molar ratios (0.95:0.05, 0.9:0.1, 0.85:0.15, 0.8:0.2, and 0.75:0.25), then put into a grinder. The powders were vibration-milled for 20 h. The products were washed with alcohol and deionized water (DI water) several times, then put in the oven at 120 ℃ for 30 min.

Field emission SEM (HITACHI-SU-5000) was performed at an acceleration voltage ranging from 0.5 to 30 kV to observe the surface morphology of the samples and measure their size, thickness, and length. At the same time, energy-dispersive spectroscopy (EDS) measurements were carried out using HORIBA E-MAX.

X-ray diffraction (XRD, Bruker D8-advance-ECO) analysis was carried out to study the structure of the powders. The relevant parameters were set as follows: light source, Cu-Kα ray (λ = 1.5406 Å); voltage, 40 kV; current, 25 mA; scanning rate, 0.2°/s; and scanning range,

20–80°. A carbon tape was affixed to the test glass and flattened, and the glass was fixed on the test stage. The test results were compared with those on the Joint Committee on Powder Diffraction Standards (JCPDS) card and diffraction peak values, and then Scherrer equation (1) was used to calculate grain size:

$$D = 0.9\lambda/\beta\cos\theta, \tag{1}$$

where D is the average grain size (nm), β is the half width (in radians), θ is the Bragg diffraction angle, and λ is the X-ray wavelength (Cu-Kα, λ = 1.5406 Å).

An ultraviolet lamp (365 nm/8 W) was used as the light source, and an ultraviolet/visible light spectrum analyzer (UV spectrophotometer, UV-1800, Shimadzu) was used to measure the concentrations of dyes, which were used to analyze the photodegradation effect. First, solutions of 400 mL of 10 ppm methylene blue and methyl orange were prepared. The dried powders were added to the dye solutions, which were then stirred with a magnetic stirrer in a dark box at room temperature for 30 min to reach an equilibrium between adsorption and desorption. Light was then irradiated on the sample, which was centrifuged every 20 min, after which the concentrations of dyes were measured with a UV-visible spectrophotometer. The degradation rate was calculated as

$$\eta = (C_0 - C)/C_0 \times 100\%, \tag{2}$$

where η is the degradation efficiency, C_0 is the initial concentration, and C is the concentration after irradiation.

3. Results and Discussion

In this experiment, a SEM system was used to observe the surfaces of the hybrid powders. Figure 1 shows SEM images of ZnO/MgO powders with different molar ratios. The particle size of the five samples was uniform and did not show significant changes; MgO was evenly distributed in the samples, and the appearance of the five samples did not differ significantly.

To determine whether the samples were mixed evenly, five different molar ratios of ZnO to MgO powders were measured by EDS, and the proportion of the number of atoms in each sample was obtained by atomic content analysis. The results are shown in Table 1. The elements zinc and oxygen each accounted for about half in a sample, and the magnesium content was much lower than expected. This may be due to instrumental limitations. The signal of magnesium is not easily detected; thus, the measurement results may be distorted, but it can still be seen that as the proportion of magnesium in the sample increased, the proportion of detected magnesium increased.

Five samples with different molar ratios were evaluated by XRD as shown in Fig. 2. According to JCPDS card 89-7746,[46] 2θ = 37.4, 43.6, 63.2, and 78.4° corresponded to magnesium oxide (111), (200), (220), and (311) planes, respectively. According to JCPDS standard card 89-1397,[47] 2θ = 31.77, 34.36, 36.37, 47.81, 57.22, 63.10, 67.20, 68.34, and 69.68°

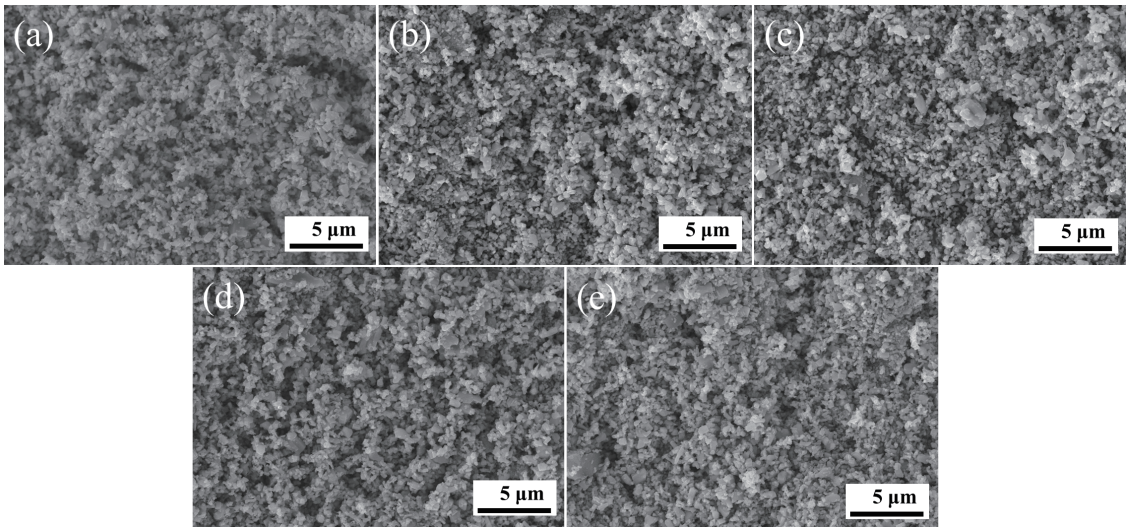

Fig. 1. SEM images of ZnO/MgO powders with different molar ratios: (a) 0.95:0.05, (b) 0.9:0.1, (c) 0.85:0.15, (d) 0.8:0.2, and (e) 0.75:0.25.

Table 1
Results of analysis by EDS of the atomic ratio of ZnO/MgO powders with different molar ratios.

Compound ratio (ZnO:MgO)	EDS (at.%, Zn:Mg:O)
0.95:0.05	57.32:0.05:46.23
0.9:0.1	53.75:0.34:45.91
0.85:0.15	52.91:0.42:46.67
0.8:0.2	52.65:0.46:46.89
0.75:0.25	58.08:0.76:41.16

corresponded to the zinc oxide (100), (002), (101), (102), (110), (103), (200), (112), and (201) planes, respectively.[48] The results show that zinc oxide has a hexagonal wurtzite structure, while the structure of magnesium oxide is unclear owing to its low content. In two powders (0.95:0.05 and 0.9:0.1) with a lower ratio of magnesium oxide, no peak of magnesium oxide was observed. The part overlapping with zinc oxide at 63° did not show the effect of the addition of powders. However, from Fig. 2, it can be seen that as the ratio of magnesium oxide continuously increased, its peak at 43° was observed in the three powders with ratios of 0.85:0.15, 0.8:0.2, and 0.75:0.25, and the experimental results are consistent with those reported in the literature.[49] The measurements were substituted into Scherrer equation (1) for calculation, and the grain size was determined to be 26, 24, 28, 28, and 23 nm for the five powders.

ZnO/MgO powders at different molar ratios were added to 10 ppm dyes at concentrations of 0.5 and 0.15 g/L; the ratios were 0.95:0.05, 0.9:0.1, 0.85:0.15, 0.8:0.2, and 0.75:0.25. Samples of the methylene blue solution were taken every 20 min and centrifuged, and the methylene blue concentration was determined to observe the methylene blue degradation. Figures 3 and 4 show the results and spectra from the degradation experiments in solutions with a methylene blue starting concentration of 0.5 g/L. The results show that methylene blue does not degrade without the photocatalyst added. The degradation rate of the sample with the 0.9:0.1 ratio is the highest,

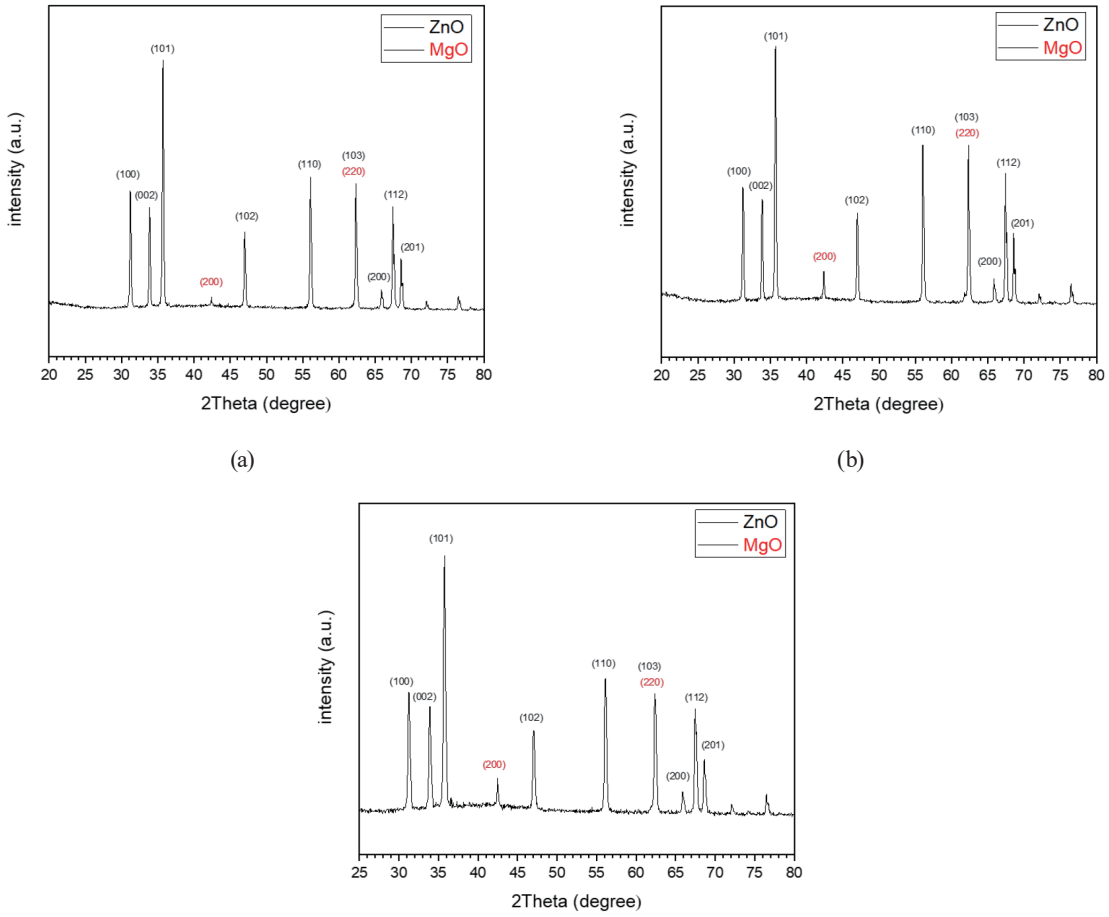

Fig. 2. (Color online) XRD results of ZnO/MgO: (a) 0.85:0.15, (b) 0.8:0.2, and (c) 0.75:0.25.

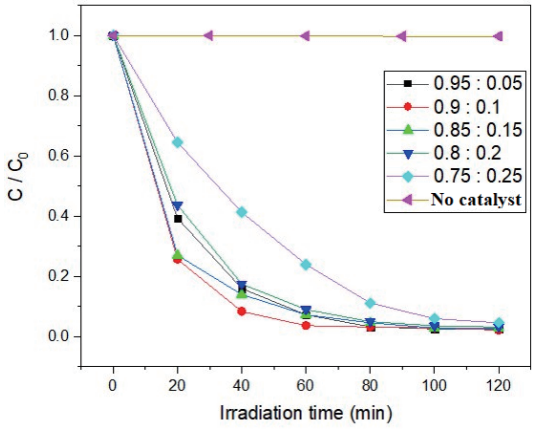

Fig. 3. (Color online) Experiments on the degradation of methylene blue by ZnO/MgO (0.5 g/L) powders at different molar ratios.

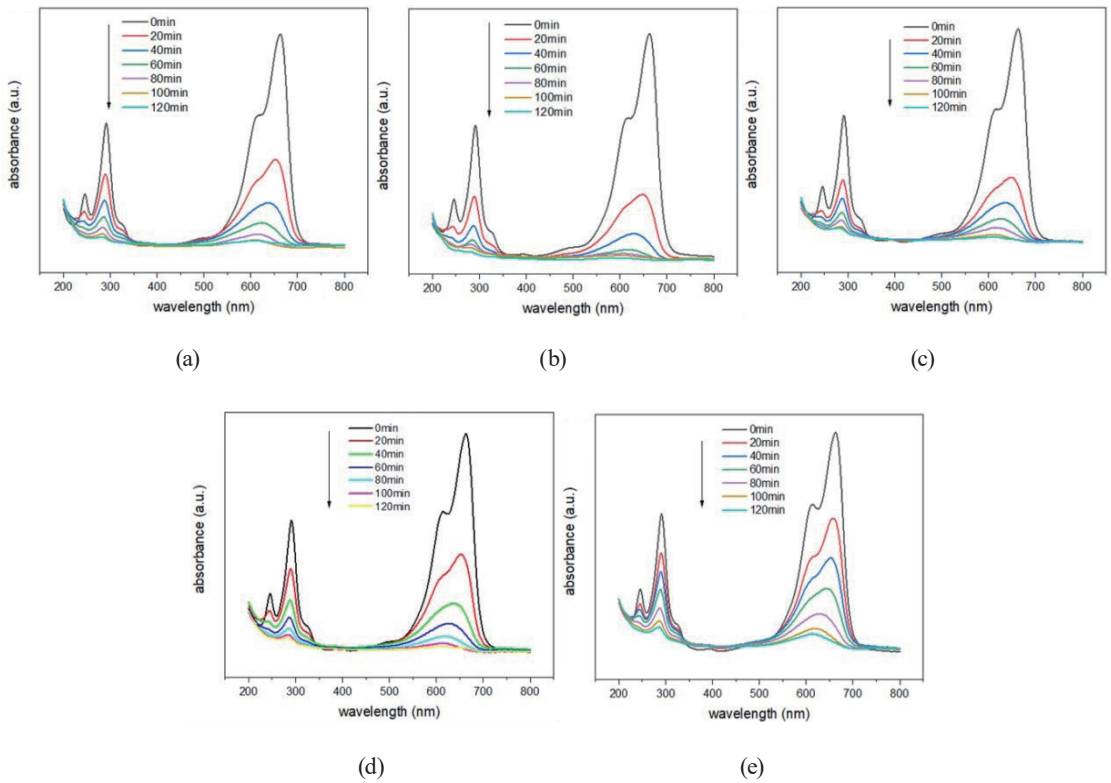

Fig. 4. (Color online) Absorption spectra of methylene blue over time as degraded by ZnO/MgO (0.5 g/L) powders at different ratios: (a) 0.95:0.05, (b) 0.9:0.1, (c) 0.85:0.15, (d) 0.8:0.2, and (e) 0.75:0.25.

and the degradation rate of the sample with 0.75:0.25 is the lowest. The five types of powders all degrade methylene blue within 2 h.

Figures 5 and 6 show the results and spectra of five powders degrading methylene blue at a concentration of 0.15 g/L. After 2 h of illumination, the 0.9:0.1 group degraded about 80%, the 0.75:0.25 group degraded about 58%, and the remaining three powders degraded between 70 and 75% of the dye.

The ZnO/MgO powders at molar ratios of 0.95:0.05, 0.9:0.1, 0.85:0.15, 0.8:0.2, and 0.75:0.25 were added to 10 ppm methyl orange solution. Samples were collected at 20 min intervals and centrifuged, and the concentration of the dye was measured to determine its degradation. Figures 7 and 8 show the results and spectra of methyl orange degraded by the five powders at a concentration of 0.5 g/L. After 3 h of illumination, methyl orange was degraded by the 0.9:0.1 powder most highly, 87% degraded by the 0.75:0.25 powder, and 95% degraded by the remaining powders.

Figures 9 and 10 show the results and spectra of methyl orange degraded by the five powders at a concentration of 0.15 g/L. After 6 h of illumination, methyl orange was totally degraded by the 0.9:0.1 powder, 75% by the 0.75:0.25 powder, and the remaining samples were degraded almost completely. The degradation rates of the three powders were 90–95%.

After the photocatalytic reaction, the ZnO/MgO powder with a molar ratio of 0.75:0.25 was recovered and used XRD to analyze the stability as shown in Fig. 11. From Fig. 11, it can be seen

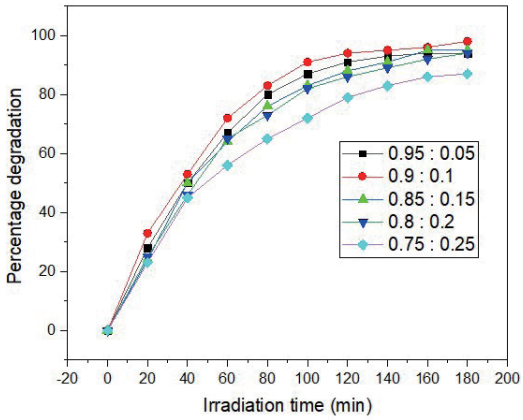

Fig. 5. (Color online) Experiments on the degradation of methylene blue by ZnO/MgO (0.15 g/L) powders at different molar ratios.

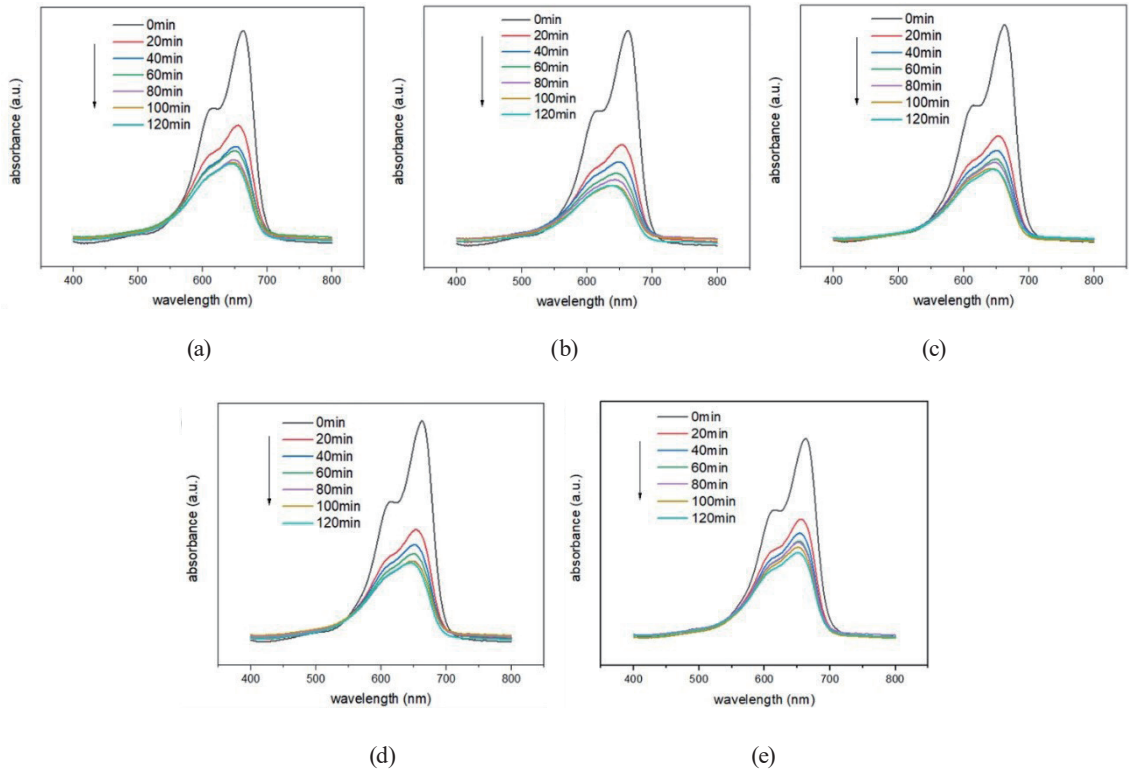

Fig. 6. (Color online) Absorption spectra of methylene blue degraded by ZnO/MgO (0.15g/L) powders at different ratios: (a) 0.95:0.05, (b) 0.9:0.1, (c) 0.85:0.15, (d) 0.8:0.2, and (e) 0.75:0.25.

that the relative size and position of the powder peaks did not change. These observations show that the powder did not participate in the reaction, and its structure was not damaged during the degradation experiment.

Photogenerated electrons and holes are excited after the photocatalyst is illuminated with adequate energy. They react with water molecules and oxygen to produce peroxides and

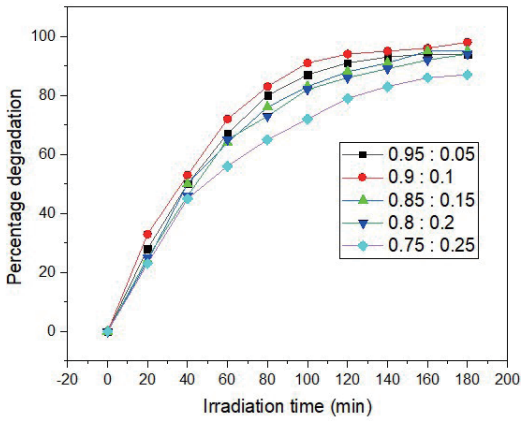

Fig. 7. (Color online) Degradation of methyl orange by ZnO/MgO (0.5 g/L) powders as a function of irradiation time.

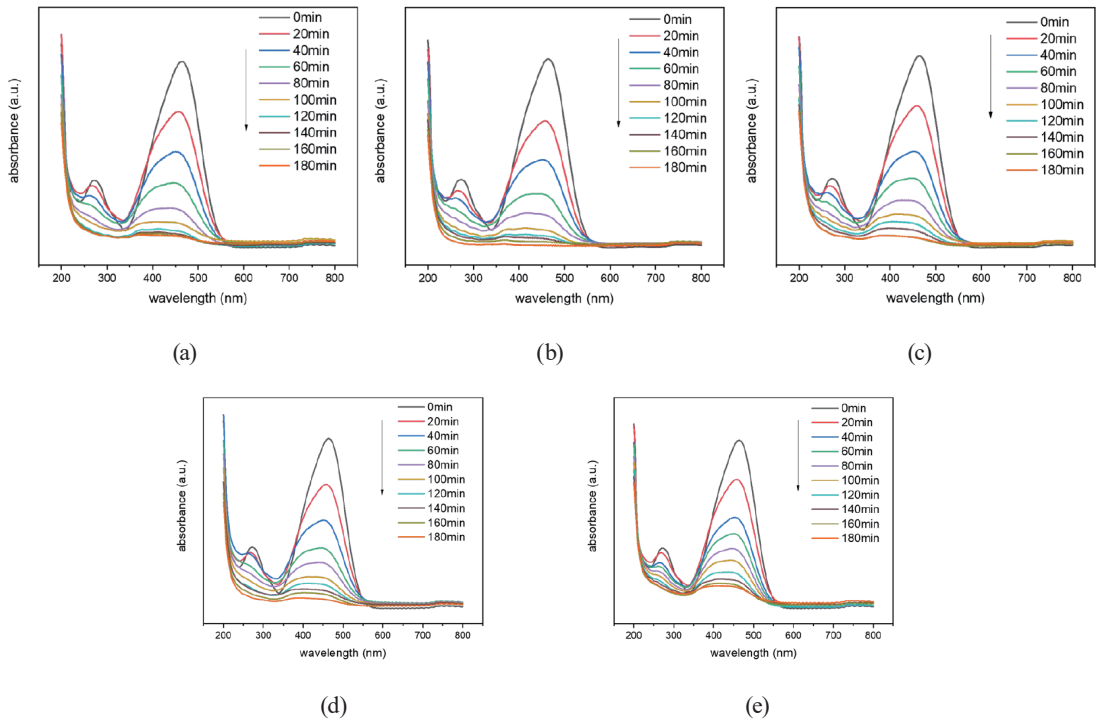

Fig. 8. (Color online) Absorption spectra of methyl orange degradation by ZnO/MgO (0.5g/L) powders as a function of time: (a) 0.95:0.05, (b) 0.9:0.1, (c) 0.85:0.15, (d) 0.8:0.2, and (e) 0.75:0.25.

hydroxyl radicals, which have powerful oxidizing and reducing capabilities, and eventually break down the pollutants in water into H_2O and CO_2 or other substances, thereby reducing the level of pollution. Figure 12 is a simplified diagram of the degradation mechanism.[50,51] When the photocatalyst is exposed to ultraviolet light, electron–hole pairs are produced on the surface of the catalyst. The photogenerated holes react with water molecules and hydroxide ions to

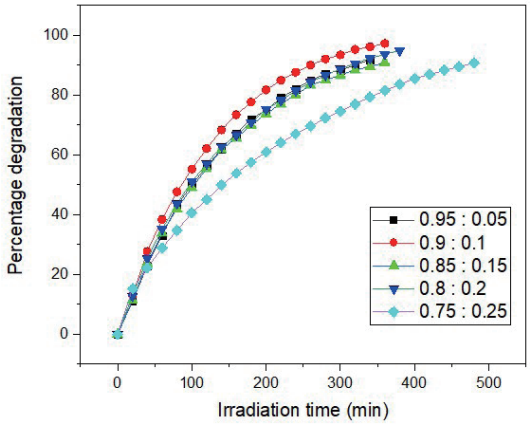

Fig. 9. (Color online) Experimental results of the degradation of methyl orange by ZnO/MgO (0.15 g/L) powders as a function of irradiation time.

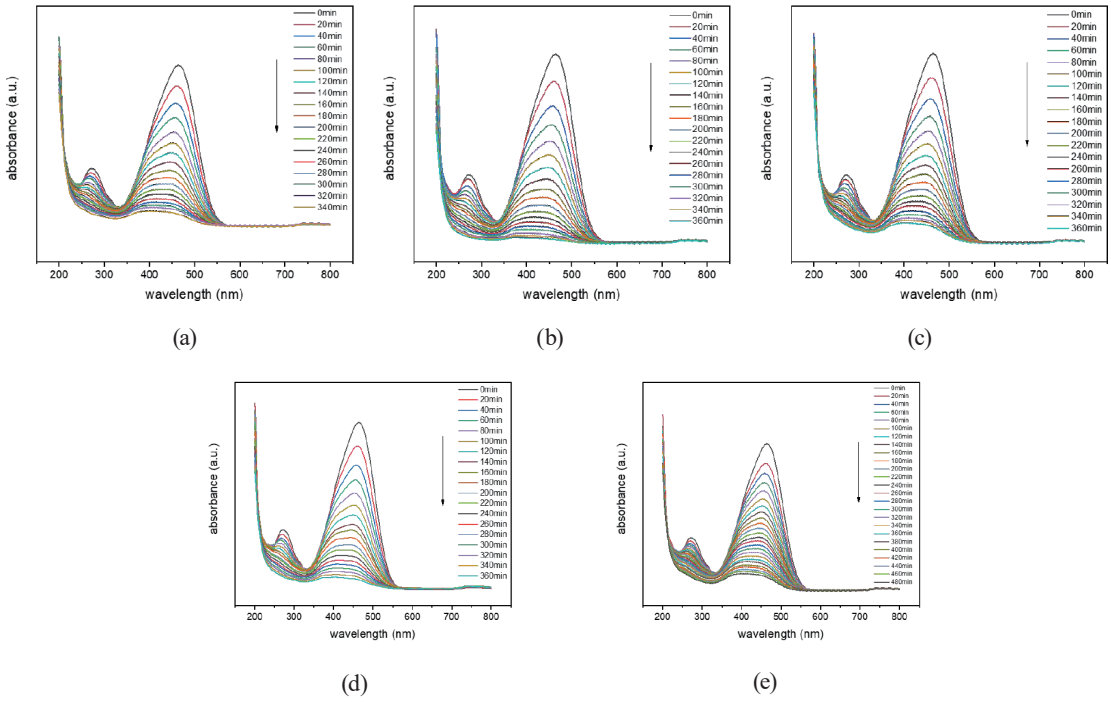

Fig. 10. (Color online) Absorption spectra of methyl orange as a function of time of degradation by ZnO/MgO (0.15 g/L) powders: (a) 0.95:0.05, (b) 0.9:0.1, (c) 0.85:0.15, (d) 0.8:0.2, and (e) 0.75:0.25.

produce hydroxyl radicals. The photogenerated electrons react with oxygen to produce negatively charged oxygen ions.[52] The negatively charged oxygen and hydrogen ions go through a series of reactions that eventually produce hydroxide ions and hydroxyl radicals. In the end, the hydroxyl radicals react with the dyes to generate a cluster of by-products, and the dyes ultimately break down into water, carbon dioxide, or other organic compounds with smaller molecular weights and thereby reduce pollution.

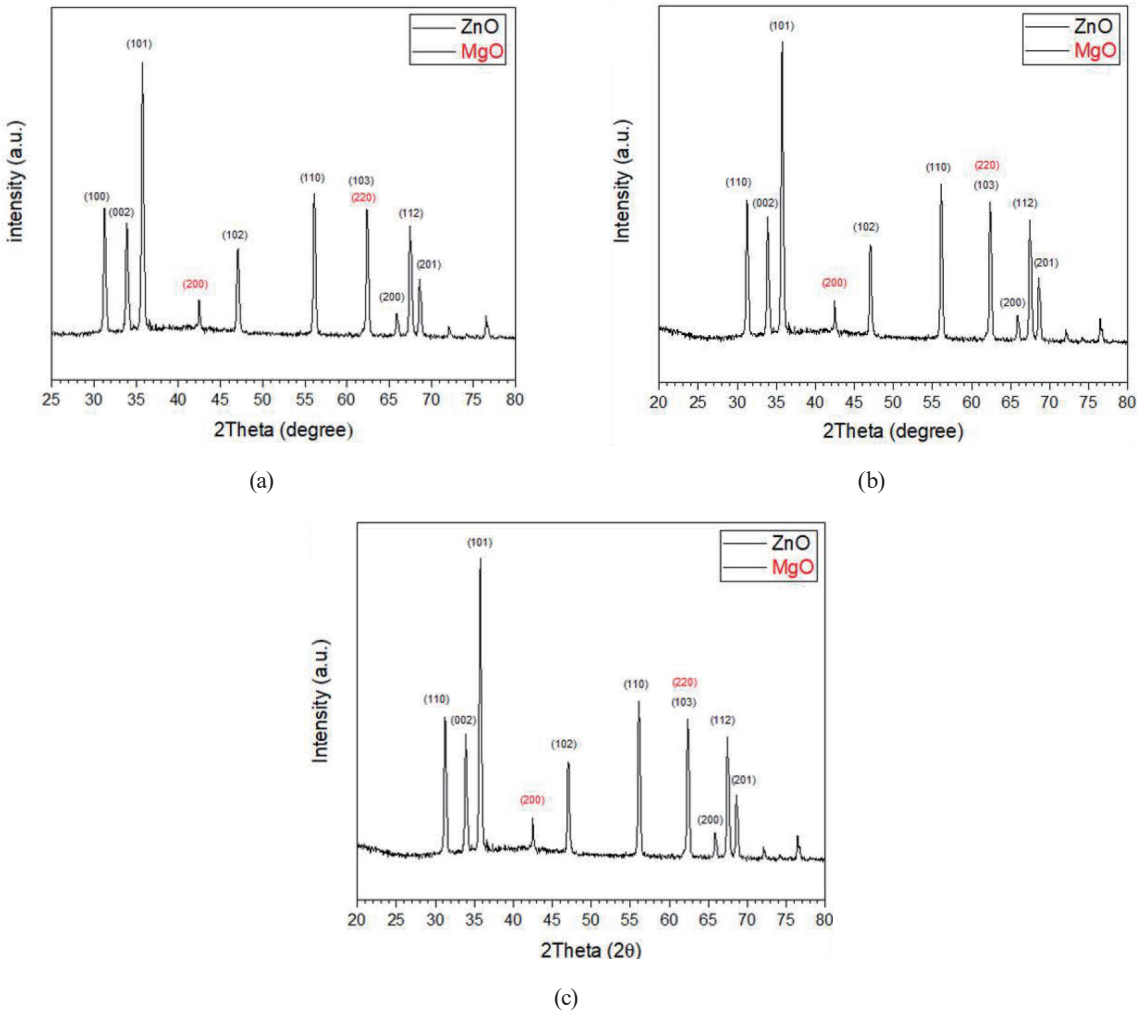

Fig. 11. (Color online) Comparison of XRD patterns of photocatalysts (a) before degradation, (b) after degradation of methylene blue, and (c) after degradation of methyl orange.

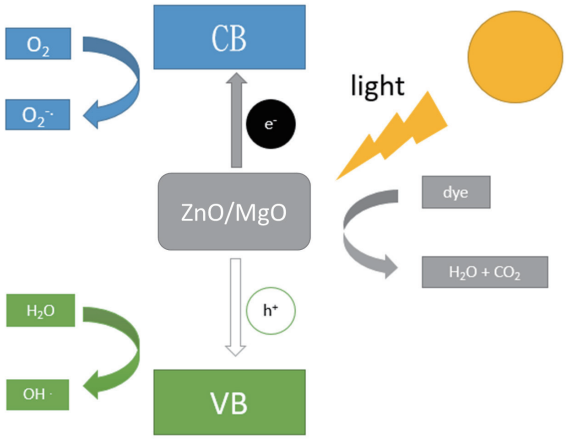

Fig. 12. (Color online) Diagram of photodegradation reactions of the ZnO/MgO photocatalyst.

4. Conclusions

In this study, zinc oxide and magnesium oxide powders were simply mixed and used to degrade methylene blue and methyl orange dyes. The best mixing ratio was determined, and the degradation effects of the powders on the two dyes were compared. The following points may be made as follows:

According to the photodegradation results, ZnO/MgO had a higher degradation rate for methylene blue, but also had a sufficient degradation rate for methyl orange with sufficient time. ZnO/MgO mixed in a molar ratio of 0.9:0.1 had the best degradation effect. The amount of MgO added was the key factor affecting the degradation efficiency.

Different proportions of powders were observed in SEM images, and no obvious difference in appearance was noted. From the distribution of atoms in EDS measurements, the powders were uniformly mixed.

The hexagonal wurtzite structure of zinc oxide was observed in XRD measurements. Among the five powders, the three with a higher proportion of magnesium oxide showed a more obvious crystalline structure of magnesium oxide as the proportion of magnesium was increased. After the reaction, the crystalline structure did not change, and the grain size of the five powders was 23–28 nm.

Acknowledgments

The authors acknowledge the support in part from the National Science and Technology Council, Taiwan, under grant number NSTC 109-2221-E-992-009-MY3.

References

1 A. Bratovčić: Technol. Acta **11** (2019) 17.
2 M. Pirilä, M. Saouabe, S. Ojala, B. Rathnayake, F. Drault, A. Valtanen, M. Huuhtanen, R. Brahmi, and R. L. Keiski: Top. Catal. **58** (2015) 1085.
3 J. Luo, W. Chen, H. Song, and J. Liu: Sci. Total Environ. **699** (2020) 134398.
4 S. Ahmed, M. G. Rasul, W. N. Martens, R. Brown, and M. A. Hashib: Water Air Soil Pollut. **215** (2011) 3.
5 Z. U. Zango, K. Jumbri, N. S. Sambudi, A. Ramli, N. H. H. Abu Bakar, B. Saad, M. N. H. Rozaini, H. A. Isiyaka, A. H. Jagaba, O. Aldaghri, and A. Sulieman: Polymers **12** (2020) 2648.
6 L. Chen, W. Zhang, J. Wang, X. Li, Y. Li, X. Hu, L. Zhao, Y. Wu, and Y. He: Green Energy Environ. **8** (2023) 283. https://doi.org/10.1016/j.gee.2021.04.009
7 S. K. Pardeshi and A. B. Patil: Sol. Energy **82** (2008) 700.
8 Y. Li, H. Chen, L. Wang, T. Wu, Y. Wu, and Y. He: Ultrason. Sonochem. **78** (2021) 105754.
9 D. Bahnemann: Sol. Energy, **77** (2004) 445.
10 M. Anpo: Catal. Surv. Asia **1** (1997) 169.
11 T. Ohno, F. Tanigawa, K. Fujihara, S. Izumi, and M. Matsumura: J. Photochem. Photobiol. A. **127** (1999) 107.
12 L. Jiang, X. Yuan, G. Zeng, X. Chen, Z. Wu, J. Liang, J. Zhang, H. Wang, and H. Wang: ACS Sustain. Chem. Eng. **5** (2017) 5831.
13 H. Wan, L. Xu, W. Q. Huang, G. F. Huang, C. N. He, J. H. Zhou, and P. Peng: Appl. Phys. A **116** (2014) 741.
14 Z. Guo, B. Sa, B. Pathak, J. Zhou, R. Ahuja, and Z. Sun: Int. J. Hydrog. Energy **39** (2014) 2042.
15 R. Shi, H. F. Ye, F. Liang, Z. Wang, K. Li, Y. Weng, Z. Lin, W. Fu, C. Che, and Y. Chen: Adv. Mater. **30** (2018) 1705941.
16 K. C. Hsu, T. H. Fang, Y. J. Hsiao, and P. C. Wu: J. Alloys Compd. **794** (2019) 576.
17 K. C. Hsu, T. H. Fang, Y. J. Hsiao, and C. A. Chan: Mater. Lett. **261** (2020) 127144.

18 K. C. Hsu, T. H. Fang, I. T. Tang, Y. J. Hsiao, and C. Y. Chen: J. Alloys Compd. **822** (2020) 153475.
19 K. C. Hsu, B. D. Chen, T. H. Fang, and C. M. Hsu: Ceram. Int. **49** (2023) 2236.
20 M. Ni, M. K. Leung, D. Y. Leung, and K. Sumathy: Renew. Sust. Energ. Rev. **11** (2007) 401.
21 G. Xie, K. Zhang, B. Guo, Q. Liu, L. Fang, and J. R. Gong: Adv. Mater. **25** (2013) 3820.
22 Y. Bessekhouad, D. Robert, J. V. Weber, and N. Chaoui: J. Photochem. Photobiol. A: Chem. **167** (2004) 49.
23 M. Radoičić, Z. Šaponjić, I. A. Janković, G. Ćirić-Marjanović, S. P. Ahrenkiel, and M. I. Čomor: Appl. Catal. B **136** (2013) 133.
24 K. C. Hsu, T. H. Fang, Y. J. Hsiao, and Z. J. Li: J. Alloys Compd. **852** (2021) 157014.
25 Y. K. Syue, K. C. Hsu, T. H. Fang, C. I. Lee, and C. J. Shih: Ceram. Int. **48** (2022) 12585.
26 W. J. Chen, K. C. Hsu, T. H. Fang, I. T. Tang, Y. J. Hsiao, and J. Y. Lin: Mater. Res. Express **6** (2019) 075905.
27 W. J. Chen, K. C. Hsu, T. H. Fang, T. H. Chen, and M. H. Li: Curr. Appl. Phys. **38** (2022) 1.
28 K. C. Hsu, T. H. Fang, S. H. Chen, and E. Y. Kuo: Ceram. Int. **45** (2019) 8744.
29 J. Kegel, I. M. Povey, and M. E. Pemble: Nano Energy **54** (2018) 409.
30 W. J. Chen, K. C. Hsu, T. H. Fang, C. I. Lee, T. H. Chen, and T. H. Hsieh: Dig. J. Nanomater. Biostruct. **6** (2021) 1227.
31 K. C. Hsu, T. H. Fang, C. I. Lee, T. H. Chen, and T. H. Hsieh: Top. Catal. **63** (2020) 956.
32 T. O. Ajiboye, O. A. Oyewo, and D. C. Onwudiwe: Surf. Interfaces **23** (2021) 100927.
33 Z. Liang, Y. Cao, Y. Li, J. Xie, N. Guo, and D. Jia: Appl. Surf. Sci. **390** (2016) 78.
34 S. Zarezadeh, A. Habibi-Yangjeh, and M. Mousavi: J. Photochem. Photobiol. A: Chem. **379** (2019) 11.
35 N. T. Hanh, N. L. M. Tri, D. Van Thuan, M. H. T. Tung, T. D. Pham, T. D. Minh, H. T. Trang, M. T. Binh, and M. V. Nguyen, J. Photochem. Photobiology. A: Chem. **382** (2019) 111923.
36 H. Zhou, J. Pan, L. Ding, Y. Tang, J. Ding, Q. Guo, T. Fan, and D. Zhang: Int. J. Hydrog. Energy **39** (2014) 16293.
37 C. Moslah, M. Kandyla, G. A. Mousdis, G. Petropoulou, and M. Ksibi: Phys. Status Solidi A **215** (2018) 1800023.
38 H. H. Mohamed and D. W. Bahnemann: Appl. Catal. B **128** (2012) 91.
39 Y. Liu, Q. Zhang, M. Xu, H. Yuan, Y. Chen, J. Zhang, K. Luo, J. Zhung, and B. You: Appl. Surf. Sci. **476** (2019) 632.
40 B. Zhang, R. Chen, Z. Yang, Y. Chen, L. Zhou, and Y. Yuan: Int. J. Hydrog. Energy **46** (2021) 508.
41 W. C. Yang, D. J. Y. Feng, H. H. Kao, M. C. Shih, M. C. Wang, C. J. Huang, and W. H. Lan: Sens. Mater. **34** (2022) 1991.
42 K. Y. Lee, A. R. Mohamed, and K. Sato: Sens. Mater. **27** (2015) 993.
43 W. He, H. K. Kim, W. G. Wamer, D. Melka, J. H. Callahan, and J. J. Yin: J. Am. Chem. Soc. **136** (2014) 750.
44 P. Panchal, D. R. Paul, A. Sharma, D. Hooda, R. Yadav, P. Meena, and S. P. Nehra: J. Photochem. Photobiol. A: Chem. **385** (2019) 112049.
45 M. Sangeeta, K. V. Karthik, R. Ravishankar, K. S. Anantharaju, H. Nagabhushana, K. Jeetendra, Y. S. Vidya, and L. Renuka: Mater. Today: Proc. **4** (2017) 11791.
46 V. T. Srisuvetha, S. L. Rayar, and G. Shanthi: Int. J. Recent Sci. Res. **5** (2018) 25.
47 L. Muñoz-Fernandez, L. S. Gomez-Villalba, O. Milošević, and M. E. Rabanal: Mater. Charact. **185** (2022) 111718.
48 V. Ravichandran, S. Sumitha, C. Y. Ning, O. Y. Xian, U. Kiew Yu, N. Paliwal, S. A. A. Shah, and M. Tripathy: Green Chem. Lett. Rev. **13** (2020) 102.
49 W. Lv, J. Yuan, B. Zhang, and Y. Wu: J. Alloys Compd. **730** (2018) 360.
50 M. N. Chong, B. Jin, C. W. Chow, and C. Saint: Water Res. **44** (2010) 2997.
51 R. Saravanan, V. K. Gupta, V. Narayanan, and A. Stephen: J. Mol. Liq. **181** (2013) 133.
52 X. G. Zheng, Q. S. Li, J. P. Zhao, D. Chen, B. Zhao, Y. J. Yang, and L. C. Zhang: Appl. Surf. Sci. **253** (2006) 2264.